Transcriptomic and Epigenetic Regulation of Disuse Atrophy and the Return to Activity in Skeletal Muscle

Fisher, A. G.[3,] *, Seaborne, R. A.[1,2] *, Hughes, T. M.[4], Gutteridge, A.[5], Stewart, C.[1], Coulson, J. M.[6], Sharples, A. P.[1,2]#, Jarvis, J. C.[2,]#

[1] Stem Cells, Ageing and Molecular Physiology Research (SCAMP) Unit, Exercise Metabolism and Adaptation Research Group (EMARG), Research Institute for Sport and Exercise Sciences, Liverpool John Moores University, Liverpool, UK.

[2] Institute for Science and Technology in Medicine (ISTM), Keele University Medical School, Keele University, Staffordshire, UK

[3] Institute for Ageing and Chronic Disease, University of Liverpool, Liverpool, UK.

[4] Instituto de Física y Astronomía, Universidad de Valparaíso, Avda. Gran Bretaña 1111, Valparaíso, Chile

[5] Pfizer, UK

[6] Cellular & Molecular Physiology, Institute of Translational Medicine, University of Liverpool, Liverpool, UK

Shortened Title: Epigenetics of Gene Expression in Muscle Atrophy

* Considered primary authors of this work

Senior Corresponding authors

#Address for correspondence:
Professor. Jonathan C. Jarvis
Research Institute for Sport & Exercise Sciences, Liverpool John Moores University,
Byrom St Campus,
Liverpool, L3 3AF, UK.
Email: J.C.Jarvis@ljmu.ac.uk

#Address for Correspondence
Dr. Adam P. Sharples
Institute for Science and Technology in Medicine, Keele University,
Guy Hilton Research Centre,
Thornburrow Drive,
Staffordshire, ST4 7QB, UK.
a.p.sharples@googlemail.com
a.p.sharples@keele.ac.uk

Abstract

Physical inactivity and disuse are major contributors to age-related muscle loss. Denervation of skeletal muscle has been previously used as a model to investigate muscle atrophy with disuse. Although gene regulatory networks that control skeletal muscle atrophy after denervation have been established, the transcriptome in response to recovery of muscle after disuse and the associated epigenetic mechanisms that may function to modulate gene expression during skeletal muscle atrophy or recovery have yet to be investigated. We report that silencing the tibialis anterior muscle in rats with Tetrodotoxin (TTX), administered to the common peroneal nerve, resulted in reductions in muscle mass of 7%, 29% and 51% with corresponding reductions in muscle fibre cross-sectional area of 18, 42, 69% following 3, 7 and 14 days of TTX respectively. Importantly, 7 days of recovery, during which rodents resumed habitual physical activity, restored muscle mass from a reduction of 51% after 14 days TTX to a reduction of only 24 % compared to sham control. Returning muscle mass to levels observed at 7 days TTX administration (-29%). Transcriptome wide analysis demonstrated that 3,714 genes were differentially expressed across all conditions at the significance level of $P \leq 0.001$ following disuse induced atrophy. Interestingly, after 7-days of recovery, the expression of genes most changed during TTX had returned towards the sham control. The 20 most differentially expressed genes following microarray analysis were identified across all conditions and cross-referenced with the most frequently occurring differentially expressed genes between conditions. This gene subset included Myogenin (MyoG), Hdac4, Ampd3, Trim63 (MuRF1) and Chrna1. Expression of these genes and Fboxo32 (MAFbx), because of its previously identified role in disuse atrophy with Trim63 (MuRF1), were confirmed by qRT-PCR and DNA methylation of their promoter regions analysed by PCR and pyrosequencing. MyoG, Trim63 (MuRF1), Fbxo32 (MAFbx) and Chrna1 showed significantly decreased DNA methylation at key time points after disuse-induced atrophy that corresponded with significantly increased gene expression. Importantly, following TTX cessation and 7 days of recovery, there was marked increase in DNA methylation profiles of Trim63 (MuRF1) and Chrna1 back toward to control levels. This also corresponded with the return of gene expression in the recovery group back to baseline expression seen in sham-operated controls. To our knowledge this is the first study to demonstrate that skeletal muscle atrophy, in response to disuse, is accompanied by dynamic epigenetic modifications that correlate with alterations in gene expression, and that these

epigenetic modifications and gene expression profiles are reversible following the return to normal activity of skeletal muscle.

Introduction

Skeletal muscle is the most abundant tissue in the mammalian body and therefore maintenance of its structure and function are important to health across the lifespan. The global maintenance of skeletal muscle mass is governed by the fine balance between muscle protein synthesis and degradation. Skeletal muscle undergoes rapid loss (atrophy) during disuse and inactivity (1-4), catabolic/inflammatory disease states such as cancer cachexia (5, 6), sepsis (7), chronic heart failure (8), obesity (9) and also with denervation following, for example, spinal cord injury (10) or during ageing (sarcopenia) (11). In order to investigate the underlying time course and mechanisms of skeletal muscle atrophy, models such as denervation via nerve section (12), tetrodotoxin (TTX) injection (13), limb suspension (14), space flight (15) and chronic overuse (16, 17) have been implemented. Within these models, large alterations in gene regulatory networks may orchestrate the altered balance between protein synthesis and degradation during muscle wasting (18). Under such conditions, these regulatory networks are altered to favour the breakdown of skeletal muscle proteins predominantly via the ubiquitin-proteasome pathway (19-21). While gene regulatory networks controlling skeletal muscle atrophy have been somewhat elucidated, the role of epigenetic alterations to modulate gene expression during skeletal muscle atrophy has received less attention. Furthermore, there are few studies investigating the transcriptomic and epigenetic change underlying the recovery of skeletal muscle following a return to normal physical activity after a period of disuse.

Epigenetic control of gene expression occurs primarily as a result of modification to DNA or chromatin/histones, as well as post-transcriptional modification of RNA (22). It has recently been suggested that denervation induced atrophy results in differential expression of genes associated with chromatin remodelling (23). Recent *in-vitro* evidence also suggests that epigenetic mechanisms may influence regeneration and myotube atrophy (24). Skeletal muscle cells that have encountered the atrophic stimulus of the inflammatory cytokine TNF-α during their early proliferative life are more susceptible to TNF-α later in their proliferative lifespan, and show impaired differentiation and regeneration compared to matched, untreated controls (24). Importantly, in this study, a retention of DNA methylation of the myogenic regulatory factor, myoD was evident over 30 population doublings in the

muscle cells receiving a single acute (24 hr) cytokine stress in early life (24). This study therefore points to a potentially important epigenetic mechanism underlying susceptibility to loss of muscle mass (25). Further, recent studies investigating 44 muscle specific genes reported that where low methylation occurred gene enhancer activity increased (26). Despite this, it has not been confirmed *in-vivo* whether the modulation of gene expression via DNA methylation is a mechanism that regulates skeletal muscle disuse atrophy.

To induce atrophy in the present study, we used tetrodotoxin (TTX) to silence the nerve to evoke disuse-induced muscle atrophy. Tetrodotoxin inhibits the firing of action potentials by binding to the voltage-gated sodium channel in nerve cell membranes, blocking the throughput of sodium ions. Therefore, the muscles innervated by the blocked nerve cannot be activated to contract (27). This model has the great advantage over nerve section, in that TTX causes a complete but reversible block of sodium channels and hence reversible nerve and muscle inactivity. In this study, in order to investigate both disuse and recovery, TTX was delivered over a pre-set period after which normal nerve activity resumed. Following nerve silencing, DNA microarray technology was used to investigate the temporal genome wide transcript expression profiles associated with progressive atrophy at 3, 7 and 14 days of disuse. The nerve block was then released, habitual activity resumed, and gene expression profiles were monitored following 7 days of recovery. Finally, DNA methylation within the promoter regions of genes was measured via pyrosequencing for genes that showed (via microarray and confirmatory qRT-PCR) the most significant alterations in expression across all conditions, and were most frequently differentially expressed when comparing between conditions. The aim of the investigation was therefore to elucidate the epigenetic control of gene expression after disuse atrophy and a return to normal physical activity in skeletal muscle, we hypothesised that: 1) disuse atrophy is controlled by differential DNA methylation that enhances or suppresses gene expression, and; 2) that DNA methylation and gene expression adaptations are transient and dynamic and therefore reversible, as normal muscle activity resumes.

Materials and Methods

Animals

Ethical approval was obtained and experimental procedures were conducted under the permissions within a project licence granted under the British Home Office Animals

(Scientific Procedures) Act 1986. Male Wistar rats weighing between 350g – 450g were housed in controlled conditions of 20 °C, 45% relative humidity with food and water available ad libitum. Animals were assigned to five groups including one control group, and three Tetrodotoxin exposed groups (TTX) for periods of 3, 7 and 14 days, including a 14 days TTX exposure plus 7-day active recovery group (recov). Experimental groups are detailed below and represented schematically in Figure 1.

Experimental Groups

The left common peroneal nerve was exposed to TTX over pre-set time courses. Groups (n = 6) consisted of 3-day (3d), 7-day (7d), 14-day (14d) TTX exposure and 14d TTX followed by 7d natural active recovery (recov). In order to control TTX exposure, a mini-osmotic pump (Mini Osmotic Pump 2002, Alzet, Cupertino CA, USA) was implanted subcutaneously in the scapular region of animals in the TTX conditions. Delivery tubes were subcutaneously channelled to a silicone rubber cuff carefully placed around the common peroneal nerve of the left hind limb. Implantation was performed in-house as a modification of a published design (28). The osmotic pump efficiently delivered 0.5 μl/hr of TTX (350 μg/ml in sterile 0.9 % saline) to the nerve cuff allowing the common peroneal nerve to be exposed to TTX, so that the ankle dorsiflexor muscles (tibialis anterior and extensor digitorum longus) were silenced but normal voluntary plantarflexion was maintained. The general welfare and mobility of the group-housed rats was minimally affected. Correct assembly and loading of the osmotic pump and nerve cuff was planned so that TTX administration would terminate after 14d, allowing recovery of hind-limb function from day 14 to day 21 within the 14d TTX + 7d recovery group.

Morphology and Histology for Muscle Size (Mass and Cross-Sectional Area)

At the end of each experimental time course, all animals were humanely euthanized with increasing CO_2 concentration and cervical dislocation, in accordance with the Animals (Scientific Procedures) Act 1986. For morphological and histological purposes, muscle was harvested from control and experimental groups ($n = 6$), weighed, divided into pieces and a transverse portion from the mid-belly of the muscle was frozen in melting isopentane, cryostat sectioned (~ 10 μm) and stained with heamatoxylin and eosin (H&E). For each muscle sample, five pictures were obtained at random. Using ImageJ 1.45i software (https://imagej.nih.gov/ij/), each photograph was overlaid with an 8 × 8 grid in to make an

unbiased selection of fibres. Ten fibres were selected for counting for each field of view at the first ten intersections of the grid that fell within a fibre. The magnification of each section was calibrated from an image of a stage graticule. Cross sectional area (CSA) was estimated from precise diameter measurements taken by selecting two points across the minimum diameter, and assuming a circular cross section. Mean tibialis anterior (TA) mass for all control and experimental groups was expressed as a percentage of whole animal body mass (428 ± 45 g) to normalise for inter-individual differences in animal size ($n = 6$) (Figure 3). Mean cross sectional area (CSA) of the TA muscle fibre was expressed as a percentage change from untreated contralateral control limb for each animal ($n = 6$) (Figure 3). All data are presented as mean ± standard deviation, unless stated otherwise.

Transcriptome Analysis

To compare genome-wide transcript expression from 3, 7, 14-d TTX and 14-d TTX plus 7-d recovery (n = 4 for each group), microarray analyses were conducted. Untreated control samples were also used for quality control of microarray analysis, and excluded from final analysis. Frozen muscle samples were sent to AROS Applied Biotechnology, where RNA was isolated via AROS Standard Operating Procedures. Over 30,000 rat transcripts and 28,000 variants were examined via Affymetrix GeneChip® Rat Genome 230 2.0 Array (Affymetrix, High Wycombe, UK). Raw data files (.CEL) were normalised via the MAS 5.0 signal method (29, 30) and .CHP files were subsequently analysed for significantly differential gene expression from microarray data (Transcriptome Analysis Console (TAC), Affymetrix, High Wycombe, UK). TAC software was used to create hierarchical clustering heatmaps of the most differentially expressed genes.

RNA Isolation and Primer Design for qRT-PCR

RNA was extracted from frozen muscle tissue (n = 6 for all sample groups) and frozen in RNA storage solution (Qiagen, Manchester UK). Samples (~ 20 mg) were immersed and homogenized in TRIzol (Thermo Fischer Scientific, UK) and RNA extracted according to manufacturer's instructions. Quantities and quality of RNA were assessed by 260/280 UV spectroscopy (Fisher, Rosklide, Denmark). Isolated RNA produced an average 260/280 ratio of 1.99 (± 0.02). Primers were designed with the Primer blast/designer (National Centre for Biotechnology Information/NCBI). All designed primers were between 20 and 21bp in length and where possible had a GC content of 50-55%. The software programme 'netprimer' predicted the efficiency of the primer products, estimating the probability of primer dimer or

hairpin formation. Primers were manufactured by Sigma and resuspended in either TE buffer or RNA free water (Sigma) as a 100 µM stock suspension. Details of primer assays are given in Table 1.

Quantitative Reverse Transcription Real Time Polymerase Chain Reaction (qRT-PCR)

Quantitative real time polymerase chain reaction (qRT-PCR) was performed by using either HotStart Taq Master Mix Kit (Qiagen, Manchester, UK) and an iQ5 Thermocycler (BioRad) or QuantiFast™ SYBR® Green RT-PCR one-step kit on a Rotorgene 3000Q (Qiagen, Manchester, UK). cDNA synthesis for subsequent PCR on the iQ5 Thermocycler was performed as follows: 1 µg of RNA was diluted in 12 µl of RNA free water and 1 µl of oligo dT primer (Invitrogen) was incubated at 70 °C for 10 mins and subsequently snap cooled on ice to enable binding of the primer. A reaction mix (4 µl of 5X buffer, 2 µl of dithiothreitol, 1 µl of deoxynucleotide triphosphates) was added per RNA samples and incubated at 42 °C for two mins. 1 µl of Superscript II Reverse Transcriptase (Invitrogen) was then added and the reaction mix incubated for a further 50-mins at 42 °C. This reaction was then inhibited by heating to 70 °C for 15 mins. As a control, reactions were prepared in parallel to those described above for each RNA sample, without the inclusion of the reverse transcriptase enzyme so that mRNA would not be reverse transcribed into cDNA. These negative control primers were used to confirm that the products amplified by PCR were indeed derived from cDNA. For qRT-PCR using HotStart Taq Master Mix Kit on the iQ5 Thermocycler, reactions were as follows; 3 µl cDNA, 15 µl Hotstar Taq Master Mix, 1.5 µl each of forward and reverse primer and 9 µl of RNAse-free water, totalling 30 µl reactions. For qRT-PCR using QuantiFast™ SYBR® Green RT-PCR one-step kit on a Rotorgene 3000Q, reactions were as follows; 9.5 µl RNA sample (7.3 ng/µl = 70 ng total RNA in the reaction), 0.15 µl forward primer, 0.15 µl reverse primer, 0.20 µl of Reverse transcriptase (RT) mix and 10 µl of SYBR® Green buffer (QuantiFast™ SYBR® Green RT-PCR one-step kit, Qiagen, Manchester, UK), totaling 20 µl. For QuantiFast™ SYBR® Green RT-PCR one-step kit, reverse transcription cycles were performed in the same tube/reaction prior to PCR, as follows: hold 50 °C for 10-min (reverse transcription/cDNA synthesis), followed by 95 °C for 5-min (transcriptase inactivation and initial denaturation step), before 40 PCR cycles of; 95 °C for 10 sec (denaturation), 60 °C for 30 sec (annealing and extension). Finally, melt curve analyses were performed to identify any primer dimer formation or non-specific amplification. All melt curves produced single reproducible melt temperatures across all

experimental samples. All relative mRNA expression was quantified using the comparative Ct ($^{\Delta\Delta Ct}$) method (31) against a known reference gene of RPIIb (polr2b) and/or Rn18s. Average Cycle threshold (Ct) values for RPIIb and Rn18s were 20.08 (±0.59) and 15.80 (±0.39) respectively across all experimental conditions.

DNA isolation and Bisulfite Conversion

To elucidate the methylation profiles, DNA was extracted from frozen muscle tissue using a commercially available DNA isolation kit (DNA Blood and Muscle Kit, Qiagen, Manchester, UK), according to that manufacturer's instructions. For methylation analysis via high resolution melt polymerase chain reaction (HRM-PCR) (see methods below), bisulfite conversion of 2 µg of DNA was performed using InnuConvert All-in-One Bisulfite Conversion kits (AJ Innuscreen GmbH, Berlin, Germany). For DNA methylation by PCR and pyrosequencing (see methods below), 500 ng of DNA was bisulfite converted using a Zymo Research EZ Methylation Kit (Cat. D5002 or D5004).

DNA methylation by Polymerase Chain Reaction and Pyrosequencing

Assays for pyrosequencing were purchased from epigenDX (Hopkinton, MA, USA) (summarised in Table 2 and Fig. 2) Following bisulfite conversion, PCR reactions were designed depending on the specific DNA methylated region of interest and the size of the product, as per manufacturer's instructions. However, a typical reaction was performed as follows; 3 µl of 10X PCR buffer (containing 15 mM $MgCl^2$), 0.2 µl of 10 mM dNTPs, 1.8 µl of 25 mM $MgCl^2$, 0.6 µl of 10 mM dNTPs, 0.15 µl HotStar Taq Polymerase, 1 µl of bisulfite treated DNA and 0.2 µM of forward and reverse primer (Table 2). One primer was biotin-labeled and HPLC purified in order to facilitate purification of the final PCR product using sepharose beads. Following an initial denaturation incubation at 95°C for 15-min, 45 cycles of denaturation at 95°C for 30 s; 63°C for 30 s (annealing), 68°C for 30 s (extension) were performed, with all PCR cycles followed by a final 5 minutes at 68°C. PCR products were then bound to Streptavidin Sepharose HP (GE Healthcare Life Sciences), after which the immobilized PCR products were purified, washed, denatured with a 0.2 µM NaOH solution and rewashed using the Pyrosequencing Vacuum Prep Tool (Pyrosequencing, Qiagen), as per the manufacturer's instructions. Following annealing with 0.5 µM sequencing primer, the purified single stranded PCR products were then sequenced using the PSQ96 HS System (Pyrosequencing, Qiagen) following the manufacturer's instructions. The methylation status of each CpG site was determined individually as an artificial C/T SNP using QCpG software

(Pyrosequencing, Qiagen). The methylation level at each CpG site was calculated as the percentage of the methylated alleles divided by the sum of all methylated and unmethylated alleles. The mean methylation level was calculated using methylation levels of all measured CpG sites within the targeted region of each gene. Each experiment included non-CpG cytosines as internal controls to detect incomplete bisulfite conversion of the input DNA. In addition, a series of unmethylated and methylated DNA strands were included as controls after each PCR. Furthermore, PCR bias testing was performed by mixing unmethylated control DNA with *in vitro* methylated DNA at different ratios (0%, 5%, 10%, 25%, 50%, 75%, and 100%), followed by bisulfite modification, PCR, and Pyrosequencing analysis. All supporting information for gene assays, including assay sequence, chromosomal CpG island locations, position from ATG start codon and transcriptional start site and CpG number are given in Table 2 and Fig. 2.

High Resolution Melting Polymerase Chain Reaction (HRM-PCR) for Total DNA Methylation

HRM-PCR for CpG methylation was performed as previously described (24). Briefly, 20 ng DNA was subjected to HRM-PCR using EpiTect HRM-PCR kits and Rotorgene 3000Q (Qiagen, Crawley, UK) with Rotorgene software (Hercules, CA, USA). All primer concentrations for gene CpG assays and EpiTect HRM master mix volumes were used in accordance with the manufacturer's instructions. HDAC4 (Qiagen) was designed to amplify a product length of 140 to 190 bp (see Table 3). PCR cycles were performed as follows; 10 s at 95 °C (denaturation), 30 s at 55 °C (annealing), 10 s at 72 °C (extension) for a maximum of 55 cycles. Following PCR, a high-resolution melt (HRM) analysis was performed with 0.1 °C increments from 65 to 95 °C. Fluorescence versus melt temperature was used to create a standard curve using rat methylated DNA standards representing 100, 75, 50, 25, 10, 5 and 0 % methylation. All samples were run in duplicate normalised to 0 % methylated control and averaged to produce a single curve. The relationship between the area under the curve, determined via each standard curve, and the corresponding percentage methylation curve of specific gene loci was determined via the best fitting fourth-order polynomial relation. This relationship was subsequently used to quantify the % methylation from the integrated raw melt curves of experimental samples. The calculations were performed using a Python-based program, MethylCal, developed for this purpose in-house (used previously in (24)).

Statistical Analyses

All statistical analyses of morphological data were performed via either; i) software R: A Language and Environment for Statistical Computing, version 2.13.1 (www.R-project.org) or, ii) a statistical package for the social sciences software for Microsoft (SPSS, version 22.0, SPSS Inc, Chicago, IL). Morphological (muscle mass and CSA) comparisons between experimental and control conditions were assessed via a one-way between groups ANOVA. Microarray data was analysed for statistical comparisons via one-way between groups ANOVA within the TAC software. Targeted qRT-PCR was analysed using a one-way between groups ANOVA (with Tukey post-hoc tests). DNA methylation data sets were analysed using a two-way between groups ANOVA (with Tukey post-hoc tests) allowing comparisons of experimental conditions and individual CpG islands. A follow up one-way ANOVA between CpG islands at each experimental condition was used to identify significant differences in DNA methylation status of each CpG island within the same experimental condition. Finally, *T*-tests were used to identify significant differences between CpG methylation in the experimental conditions and control. All statistical analysis for DNA methylation was performed on absolute values, with figures representing data as mean fold change (± standard deviation) to relevant control. Differences were considered statistically significant when $P \leq 0.05$.

RESULTS

Skeletal Muscle Disuse and Recovery evokes Considerable yet Reversible Muscle Atrophy

Exposure to TTX produced an average of 7.0 ± 2.4% loss in TA muscle mass at 3-d, 28.7 ± 5.1% at 7-d and 50.7 ± 2.7% loss following 14-d that resulted in statistical significance at all time points versus the unoperated right TA ($P < 0.001$; Fig. 3) and a significant difference between paired comparisons of 3 and 7-d, 3 and 14-d, 7 and 14-d ($P < 0.001$). After 14 d TTX exposure followed by 7d cessation in recovery group, muscle mass significantly recovered by 51.7% vs. 14 d of denervation ($P = 0.001$; Fig. 3). Seven days of recovery did not completely restore muscle mass, as muscle mass was still significantly lower than control ($P < 0.001$; Fig. 3), total muscle mass was equivalent to levels at 7-d TTX administration, suggesting that rates of loss over 7-d were similar to rates of recovery. We therefore report significant skeletal muscle atrophy of the TA muscles with disuse and a 51.7% recovery of muscle mass following 7-day cessation of the TTX administration and return of normal habitual physical activity.

Exposure to TTX produced a progressive reduction in mean muscle fibre CSA of 17.95 ± 12.06% at 3-d, 42.09 ± 6.17% at 7d and 68.94 ± 2.97% at 14-d of TTX exposure, with 7-d and 14-d TTX exposure being significantly reduced versus the control ($P = 0.003$; $P < 0.001$, respectively; Fig. 4). Similarly, to TA muscle mass, upon TTX cessation, the 14-d TTX + 7-d recovery group muscle CSA significantly recovered compared to 14-d TTX alone, with an increase of 62.6% in CSA compared with 14-d TTX alone ($p = 0.002$; Fig 4). Therefore, there was significant atrophy of individual skeletal muscle fibres in the TA muscles following denervation and a 51.7% recovery of muscle mass and 62.6% recovery of muscle CSA following 7-day cessation of the TTX administration and normal habitual physical activity.

Gene Expression Microarrays Identify Important Gene Regulatory Networks involved in Muscle Atrophy and Recovery.

After confirming significant reduction in muscle mass, the temporal transcriptome profile accompanying muscle atrophy was investigated (n=4). The dendogram from hierarchical clustering of probe sets across the genome identified 3,714 genes that showed highly significant differential expression with a P value of ≤ 0.001 (Fig. 5a). It also demonstrated that there was a strong clustering of data for the 3, 7 and 14-d TTX groups, which were clearly separated from another identified clustering of data consisting of the sham-operated control and the recovery groups (Figure 5a and Supp. 1a). This suggested that disuse-induced atrophy evoked a considerable characteristic change in expression of a large number of genes that were returned back to levels in the sham controls on cessation of the nerve block in the recovery group (Fig. 5a). Despite the top 20 genes showing recovery back to control sham levels, 846 genes were still significantly differentially expressed ($P < 0.05$) in the recovery group compared to sham control (Supp. 1i). Further analyses were performed using unsupervised hierarchical clustering of the top 20 most differentially expressed genes (Fig. 5b and Supp. 2). This analysis confirmed that these top 20 genes most differentially expressed in TTX groups returned back towards sham control following 7 days of recovery. Furthermore, the top 500 genes that were upregulated by TTX administration could be grouped into three distinct clusters based on their temporal behaviour: An immediate and sustained increase in expression (Fig. 5c), a delayed but progressive increase in expression (Fig 5d), and finally an immediate increase in expression that declined over the time course (Fig 5e), suggesting that dynamic disuse and co-ordinated gene expression occurred across a large number of genes as a result of disuse and the return back towards control levels in the recovery group.

This suggested that disuse-induced atrophy evoked a considerable characteristic change in expression of a large number of genes that were returned back to levels in the sham controls on cessation of the nerve block in the recovery group (Fig. 5a). Further analyses were performed using unsupervised hierarchical clustering of the top 20 most differentially expressed genes (Fig. 5b and Suppl. 1b). This analysis confirmed that these top 20 genes most differentially expressed in TTX groups returned back towards sham control following 7 days of recovery. Furthermore, the top 500 genes that were upregulated by TTX administration could be grouped into three distinct clusters based on their temporal behaviour: An immediate and sustained increase in expression (Fig. 5c), a delayed but progressive increase in expression (Fig 5d), and finally an immediate increase in expression that declined over the time course (Fig 5e), suggesting that dynamic disuse and co-ordinated gene expression occurred across a large number of genes as a result of disuse and the return back towards control levels in the recovery group.

Regulated Genes Identified by Microarray and Ranked by Significance of Change

Transcriptome wide data was analysed to compare between conditions in 6 pairwise comparisons (Sham vs. 3d (Suppl. 1c), 7d (Suppl. 1d), 14d (Suppl 1e) and Recovery vs. 3d (Suppl. 1f), 7d (Suppl. 1g), 14d (Suppl. 1h)) to identify the genes that were among the most significantly affected in the experimental groups. Trim 63 (MuRF1), Myogenin (MyoG) and Ampd3 were identified as being the most frequently occurring genes most differentially expressed across these paired comparisons, that also appeared in the top 20 differentially expressed genes across all conditions (Fig. 5b and Supp. 1b). Ampd3 appeared in 4 out of 6 of these paired comparisons (Supp 1c, 1f, 1g, 1h). Previous studies have also suggested overexpression of Ampd3 increases protein degradation in C2C12 myotubes (32), and thus we sought to further elucidate its transcriptional and epigenetic role in denervation induced atrophy in the present manuscript. The E3 ubiquitin ligase, Trim 63, appeared in 3 out of 6 paired comparisons (Suppl. 1c, 1f, 1h) and has been previously strongly associated with muscle atrophy *in-vitro* and *in-vivo* (33-37), as is its protein family member, Fbxo 32 (Mafbx). We therefore extended the analysis of this change by qRT-PCR and loci-specific pyrosequencing for DNA methylations role in TTX-induced atrophy and recovery. The muscle specific basic helix-loop-helix (bHLH) myogenic regulatory factor, MyoG, was also identified in 3 out of 6 paired comparisons (Suppl. 1c, 1d, 1e) and has also previously been identified as a key transcript in regulating denervation-dependent muscular atrophy in rodent

models (38). Importantly, the class II histone deacytelase (Hdac 4), also appeared within the top 20 most statistically differentially expressed genes across all probe sets (Fig. 5b, Suppl. 1b), and was the most statistically differentially expressed gene when comparing sham control to 3D TTX atrophy probe sets (Suppl. 1c). Hdac 4 is a known upstream regulatory factor of MyoG activity (36, 39), and thus both Hdac 4 and MyoG genes were identified as warranting further targeted analysis. Additional NMJ associated genes that were significantly altered and appeared in the top 20 most differentially expressed genes included the acetylcholine receptor subunit alpha 1 (Chrna1) (Figure 5b). This gene also appeared in 2 out of 6 paired comparisons of most differentially expressed genes (Suppl. 1d, 1e). Chrna1 plays a crucial role in acetylcholine binding and channel gating activity, within the neuromuscular junction pathway (40) and has been previously been identified via transcriptome analysis as the most differentially expressed gene in skeletal muscle loss observed in age related muscle loss/denervation (41). After identification of key gene transcripts, quantification of gene expression was elucidated via follow up qRT-PCr in order to confirm and further profile the transcriptional responses and DNA methylation analyses were performed with pyrosequencing to assess the status of the genes promoter region in response to disuse muscle atrophy and recovery.

Changes in Gene Expression Following Disuse Induced Atrophy Are Returned to Control Levels Following Recovery

Confirmation of microarray gene expression by qRT-PCR demonstrated that of MyoG, Hdac4 Trim63 and Fbxo32 significantly increased at 3d of TTX exposure compared to control ($P < 0.05$), with Hdac4 and Fbxo32 (Fig. 6a) remaining elevated at 7d of TTX exposure. By 14d the mean levels for Hdac4, MyoG, Trim63 and, Fbxo32 were not significantly different, suggesting elevation predominately at 3-7 days of these genes in response to disuse. In contrast, while significant changes in Ampd3 expression were not detected (Fig. 6a), Chrna1 expression was significantly elevated at 3, 7, and 14 days (177.5-fold increase vs. control; $P = 0.016$, Figure 6a). Following TTX cessation and 7 days of recovery; Hdac4, MyoG, Trim63, Fbxo32 and Chrna1 gene expression had all returned to Sham control levels, as suggested above in the microarray data.

DNA Methylation Regulates Gene Expression involved in Disuse Induced Atrophy and Recovery

Loci-specific pyrosequencing of individual CpG islands within gene promoters revealed

significant alterations in the DNA methylation of the key genes identified following microarray analysis and confirmatory qRT-PCR, that corresponded with significant increases in gene transcription. Following 3-d TTX exposure, there was a significant reduction (P=0.011) in DNA methylation of the MyoG gene promoter (Fig. 6b) and a concomitant significant increase (P=0.011) in myoG gene expression (Fig. 6a), both of which then returned towards baseline levels over the remaining 14 days (all gene expression/DNA methylation overlap relationships are schematically represented in Fig 6c). The DNA methylation profile of the Chrna1 gene promoter progressively decreased relative to control, with 7-d and 14-d TTX treatment attaining significance versus sham controls ($P = 0.035$; $P < 0.001$, respectively). This corresponded with the increased expression of this gene over the 14-day denervation period (Fig. 6a and 6c). Like Chrna1, Trim63 displayed significant reduction in methylation at 7-d and 14-d of TTX exposure ($P = 0.035$; $P < 0.001$, respectively), (Fig. 6b and 6c) which coincided with a stable increase in mRNA expression at the same time points (Fig. 6a and 6c). Fbxo32 showed a decreasing trend in DNA methylation at specific time points, attaining significance at 14-d TTX exposure ($P = 0.021$) (Fig. 6b, 6c), with gene expression data reporting significant increases at 3-d ($P = 0.037$) and 7-d ($P = 0.038$) atrophy (Fig 6a, 6c). Importantly, following TTX cessation there was a recovery in the DNA methylation profile in Trim63, Fbxo32 and Chrna1 returning to sham control levels ($P > 0.05$). This was in conjunction with an observed recovery of gene expression of the same genes upon TTX cessation (Fig 6c). We found no differences in DNA methylation for Ampd3 following TTX administration or recovery (Fig. 6b). Furthermore, following initial total % of methylation within the total amplicon/product via HRM PCR for Hdac4 we were unable to identify methylation above that of the 0% methylation control for all conditions and therefore pyrosequencing for loci specific DNA methylation was not performed for Hdac4.

Discussion

Summary

The aim of this investigation was to elucidate the epigenetic control of gene expression following skeletal muscle disuse atrophy following 3, 7 and 14 days of nerve block with TTX. Firstly, we found a 7, 29 and 51% loss of muscle at 3,7 and 14 days of disuse, with 7 days of recovery resulting in a 51.7% restoration of total muscle mass lost after 14 days of disuse. Muscle mass was therefore similar after 7 d of disuse or 14d of disuse followed by 7 d

of normal activity. Muscle atrophy was further confirmed with fibre cross-sectional area data, in which a similar pattern of progressive loss was observed of 18, 42, 69% following 3, 7 and 14 days of TTX respectively. Seven days of recovery, restored 63% of muscle cross-sectional area vs. 14-day disuse atrophy alone. Our original hypothesis was supported, in that disuse atrophy was associated with reduced DNA methylation and enhanced expression of a sample genes whose expression was most affected by disuse and recovery. Both DNA methylation and gene expression were partially returned to baseline after 7 days of recovery from the nerve block. Importantly, following gene expression microarray analysis we found that 3,714 genes were highly ($P \leq 0.001$) significantly regulated in TTX groups, and that these genes were returned in the recovery group back towards levels observed in the sham control. Specifically, by identifying the top 20 most differentially expressed genes in atrophy and recovery groups, and cross referencing with the most frequently occurring significantly regulated genes for between group pairwise comparisons, we identified a key subset of influential genes MyoG, Hdac4, Trim63 (Murf1), Ampd3 and Chrna1. These genes, together with Fboxo32 (Mafbx) because of its previously defined role with Trim63 (Murf1) in muscle atrophy (discussed below), were then analysed via qRT-PCR to confirm microarray gene expression data for these genes as well as loci-specific DNA methylation of the promoter regions by pyrosequencing. All these genes (MyoG, Hdac4, Trim63/Murf1, Ampd3, Chrna1 and Fboxo32/Mafbx) have been identified previously via transcriptome wide analysis of disuse atrophy following neuromuscular blocker α-cobrotoxin treatment (42). In this investigation, we showed novel data suggesting that MyoG, Trim63 (Murf1), Fbxo32 (Mafbx) and Chrna1 had reduced DNA methylation at specific time points following disuse induced atrophy that corresponded with time dependent increases in gene expression. Importantly, following TTX cessation and 7 days of recovery during which normal habitual physical activity was resumed, there was a return of DNA methylation for Trim63, Fbxo32 and Chrna1, back towards sham control levels. Importantly, this also corresponded with the return of gene expression back to that of baseline sham controls. As reduced DNA methylation within promoter or enhancer regions of genes can lead to enhanced gene expression because reduced methylation allows access for RNA polymerase to enable transcription (43), our data suggests that atrophy and recovery of skeletal muscle following disuse is associated with dynamic and transient epigenetic modifications that correspond with altered gene expression.

Dynamic and Transient DNA Methylation following Atrophy and Recovery of Muscle Mass.

Interestingly, 51.7% of total muscle mass loss after 14 days was restored following 7 days of recovery, yet importantly gene expression was returned fully to baseline after 7 days, suggesting, as perhaps would be expected due to the time required for transcription, translation and protein incorporation, a time lag between gene expression and physiological restoration of muscle mass. However, the findings in this study suggest that the reduced DNA methylation corresponding with increased gene expression of MyoG, Trim63 (MuRF1), Fbxo32 (MAFbx) and Chrna1 is a dynamic and transient event, in which decreases in DNA methylation at 3, 7 and 14 days of TTX-induced atrophy correspond with increases in gene expression, that in turn are returned back to baseline (Trim63/MuRF1) and Chrna1) within just 7 days after the removal of the TTX block. DNA methylation has previously been reported to be mitotically stable and as such, environmental factors were believed to be unable to induce significant alterations in DNA methylation at both acute and chronic time points (44). Furthermore, our previous data suggests that even following acute catabolic stress, DNA methylation can be stably retained across several population doublings of muscle cells *in-vitro* (24). However, we show here that DNA methylation does respond at a rate that allows for its participation in the adaptive control of gene expression, and adds further support to previous findings of transient alterations of skeletal muscle DNA methylation, for example following acute aerobic exercise (24, 45). Our data adds further support to previous findings of transient alterations of skeletal muscle DNA methylation.

Although not identified in this study it will be important in future studies to investigate DNA methyltransferase activity. The de novo methyltransferases (DNMT 3a, 3b) are involved in the initial incorporation of methyl groups to cytosine residues and the creation of 5-methylcytoseines (5-mC) to increase in DNA methylation. The maintenance DNA methyltransferase (DNMT 1) is involved in retaining the methyl tag onto the DNA strand (46). The dynamic and transient observation of DNA methylation in this study is suggestive of a high activity of DNMT 3a and 3b activity in which initial and rapid increases in DNA methylation is observed. However, we do not report significant retention of DNA methylation upon TTX cessation (14-d TTX + 7-d recovery), which would suggest that DNMT 1 has not maintained the methylation status of some of these genes beyond muscle recovery. It has previously been reported that increases in both types of DNMT is observed following a high-fat diet that induced increases in DNA methylation of 6,508 genes (47). Further work is needed to confirm similar findings in atrophying muscle, and to elucidate the

response of DNA methyltransferases upon the reversible insult. Finally, it would be important to undertake 14 d recovery in future experimentation to assess whether muscle mass can be returned fully back to baseline control levels and to examine the transcriptomic and epigenetic responses during this period.

DNA Methylation Correlates with Important Changes in Skeletal Muscle Gene Expression following Disuse-Induced Atrophy and with the Return of Gene Expression to Baseline during Recovery.

As suggested above: MyoG, Trim63, Fbxo32 and Chrna1 showed decreased DNA methylation following disuse-induced atrophy that corresponded with increased gene expression. Importantly, following TTX cessation and 7 days of recovery during which normal habitual physical activity was resumed, Trim63 and Chrna1, TTX-induced DNA methylation returned back to control levels as repression of gene expression recovered. The muscle specific basic helix-loop-helix (bHLH) transcriptional factor and member of the myogenic regulatory factors (MRFs), MyoG is commonly associated with the coordination of skeletal muscle development/myogenesis or skeletal muscle regeneration, and specifically the differentiation/fusion of skeletal muscle cells (48). Here we report a significant induction of gene expression for this transcription factor upon disuse-induced muscle atrophy. Because expression of this protein is usually associated with muscle regeneration, this may reflect a compensatory mechanism in an unsuccessful attempt to halt atrophy or to respond to a return of activity. The role of MyoG as a transcription factor has previously been linked with the regulation of the ubiquitin E3 ligases, Trim63 and Fbxo32 and associated muscle atrophy (34). Importantly, we provide novel data that suggests the DNA methylation profile of this transcript is altered in an inverse fashion to its mRNA expression. Indeed, at 3, 7 and 14 d we saw a significant reduction in MyoG DNA methylation and an increase in MyoG transcript expression. We therefore suggest that increased MyoG gene expression is regulated by reduced MyoG DNA methylation.

Previous studies have also reported that MyoG gene expression is under the regulatory control of class II histone deacetylases (Hdacs) (34, 35). In partial support of this notion, we report a significant increase in class II Hdac, Hdac4 gene expression at 3 and 14-d of TTX exposure. We did not however, measure protein abundance or phosphorylation/ deacetylation status of Hdac4. Indeed, initial screening of Hdac 4 DNA methylation through HRM PCR

was unable to detect a notable change, with global gene percent methylation showing no greater values than 0 % methylated controls. Therefore, further work at the protein and histone level is needed to elucidate the epigenetic regulation of Hdac's during periods of loss and recovery of muscle mass, as its altered gene expression following denervation does not seem to be controlled via DNA methylation. Furthermore, despite a return of MyoG gene expression back to control levels following 7-days recovery, DNA methylation continued to reduce in the recovery group. This shows that while reduced DNA methylation may have been important in increased gene expression during denervation induced atrophy, that DNA methylation was not controlling gene expression of MyoG during recovery.

As suggested above, down-stream transcriptional targets of MyoG have also been shown to be highly induced during periods of muscle loss caused by denervation, immobilization and un-loading in rodents (49, 50). Trim63 is an E3 ubiquitin ligase and a member of the RING zinc finger family of proteins, that directs the polyubiquitination of proteins to target them for proteolysis. With catabolic stimuli, such as diabetes, cancer, denervation, unloading and glucocorticoid or cytokine treatment, its expression has consistently been shown to increase (50, 51). Previous studies have also suggested that upon denervation, northern blot analysis shows a significant increase in Trim63 and Fbxo32 following 3 days of muscle atrophy and continuing through to 7-d (50). Here, we report a significant increase in Trim63 and Fbxo32 gene expression via qRT-PCR compared to control levels, at the same time as a reduction in DNA methylation. Importantly, this suggests an important role for epigenetic control of these ubiquitin ligases, in the resulting protein degradation and muscle loss observed in this study. We note that DNA methylation of both of these ubiquitin ligases increased back towards control levels with corresponding decreases in gene expression back towards the sham control level, suggesting that the reductions in DNA methylation during atrophy can be dynamically regulated.

Further, the acetylcholine receptor subunit alpha 1 (Chrna1) makes up the majority of the muscle specific nicotinic acetyl choline receptor (nAchR) in adult skeletal muscle (52) and plays a crucial role in initiating the opening of the nAchR channel and the transfer of positively charged ions (53). Interestingly, we report a progressive increase in gene expression with a cumulative significant fold change exhibited by 14-d of TTX exposure. This alteration in gene expression is met with a parallel progressive reduction in DNA methylation with significance being observed at both 7 and 14-d following TTX-induced

atrophy. We report similar results to previous work (54), in which a significant increase in Chrna1 activity was also observed during sarcopenia induced atrophy. The nAchR are made up of 5 isoforms in human skeletal muscle, in with the subunit 1 alpha (Chrna1) is most dominant. These isoforms function to create an acetylcholine cluster around the neuromuscular central pore, in which they house target binding sites predominantly located at the alpha subunit in the extracellular domain near the N terminus. Upon contact of a chemical messenger to the binding site, all present subunits undergo a conformational change resulting in the nAchR channel opening (55). Upon denervation, however, no action potential messages are received and therefore it is possible that the reduced DNA methylation and increased transcriptional response (although we do not provide evidence of protein levels) may increase as a compensatory mechanism understood to increase the chance of forming new end plates. This response is equivalent to that seen after nerve section and it appears therefore to be a response to lack of activity rather than physical absence or damage to the nerve. Finally, upon TTX cessation and muscle recovery we report a return to control of the DNA methylation signature, coupled with a return to control of gene expression. Finally, as discussed above, genes such as MyoG, ubiquitin ligases, and Chrna1 have been identified as major regulators of muscle regeneration, protein degradation and function respectively. As the present study also identified these genes as being the most frequently occurring differentially expressed genes across comparisons using a non-selective transcriptome wide approach in a novel model of osmotically administered TTX-induced atrophy, further consolidates the important role of these genes in disuse atrophy.

Conclusion

MyoG, Trim63, Fbxo32 and Chrna1, but not Ampd3, showed decreased DNA methylation following disuse-induced atrophy that corresponded with increased gene expression and muscle atrophy. Importantly, following TTX cessation and 7 days recovery, there was increased DNA methylation of Trim63 and Chrna1 back toward to control levels, that also corresponded with the return of gene expression back to that of baseline in sham controls. Overall, this suggests that atrophy and recovery of skeletal muscle following disuse is in part controlled by dynamic and transient epigenetic regulation of gene expression.

Acknowledgments

Fisher, AG (via Jarvis, JC) were supported for this work through an integrative mammalian biology studentship from the Medical Research Council (MRC), UK. Seaborne, RA (via

635 Sharples AP) were supported for this work via a Doctoral Training Alliance funded
636 studentship and GlaxoSmithKline.
637
638 **Author Contributions** Fisher, A., Seaborne, R.A., Coulson, J.M., Sharples, A.P., Jarvis J.C.
639 designed research; Fisher, A., Seaborne, R.A., Hughes, T.M., Gutteridge, A., Stewart C.E.,
640 Coulson, J.M., Sharples, A.P., Jarvis, J.C., analysed data; Fisher, A., Seaborne, R.A, Coulson,
641 J.M., Sharples, A.P., Jarvis, J.C., performed research; Seaborne, R., Fisher, A., Stewart C.E.,
642 Sharples, A.P., and Jarvis JC wrote the paper; Hughes, T.M., contributed analytic tools.
643
644
645
646 **Figure Legends**
647
648 **Figure 1. Schematic Representation of the TTX Muscle Atrophy Model and Subsequent**
649 **Muscle Sample Preparation for Morphological, Transcriptomic and Epigenetic**
650 **Analysis.** (A) Display of physiological location of tetrodotoxin administration pump. Inset
651 shows; i) real image of osmotic pump location and assembly within the left hind limb of the
652 rodent and, ii) provides a representation overview of the osmotic pump assembly, black lines
653 show osmotic pump unit and delivery tube to nerve cuff unit and white line displays the
654 synaptic nerve. (B) Muscle sample preparation for downstream analysis: Left (treated), right
655 (untreated contralateral control), n=6.

656 **Figure 2. Gene map of CpG Islands for Loci Specific Pyrosequencing for Quantification**
657 **of DNA Methylation Pyrosequencing.** In descending order: Myogenin (myog), Fboxo32
658 (MAFbx), Trim63 (MuRF1), Ampd3, Chrna1.
659
660 **Figure 3. Quantification of Muscle Atrophy (muscle mass) *in-vivo* following TTX-**
661 **Induced Nerve Block.** Data shown for 3, 7 and 14 day treatment, and TTX nerve block + 7
662 Day active recovery (7-d Recovery). Mean tibialis anterior (TA) mass for all control and
663 experimental groups were expressed as a percentage difference of whole animal body mass
664 (428 ± 45 g) to normalise for inter-individual differences in animal size (A), All data
665 presented as mean ± standard deviation for n=6 in each condition. All statistical significance
666 (via Pairwise Tukey post-hoc test) represented via *, with experimental conditions showing

significance relative to sham control, and 7d-recovery showing significance to 14-d TTX alone, indicated via #. All statistical values detailed in results text.

Figure 4. Muscle Fibre Cross Sectional Area (CSA) after TTX-induced Atrophy and Recovery. Graphed figure represents Mean cross sectional area (CSA) of the TA muscle was expressed as a percentage change from untreated contralateral control limb for each animal. Haematoxylin and eosin stained sections of untreated (A) and treated (B) tibialis anterior muscle of control (i), 3-day TTX exposed (ii), 7-day TTX exposed (iii), 14-day TTX exposed (iv), 14-day TTX exposed with 7-day recovery (v). All statistical significance (via Pairwise Tukey post-hoc test) represented via *, with experimental conditions showing significance relative to sham control, and 7d-recovery showing significance to 14-d TTX alone, indicated via #. All statistical values detailed in results text.

Figure 5. Genome Wide Transcript Expression Indicates Highly Dynamic Response to Progressive Muscular Atrophy that Returns to Sham Control Upon Muscle Recovery. Hierarchical clustering heatmaps of probe set expression across the rodent genome identifies 3,714 genes that are highly statistically significantly (P value of ≤ 0.001) expressed across all conditions, with 3, 7 and 14D TTX atrophy being differentially expressed in comparison to sham control and 14D TTX + 7D recovery (A). This observation is confirmed in the top 20 statistically differentially expressed genes across all conditions with distinct clustering occurring, suggesting significant differences in the expression of probe sets of 3, 7 and 14 day TTX compared to sham control and 14 day TTX + 7D recovery (B). Top 500 most statistically differentially expressed genes grouped into three distinct clusters i) an immediate and sustained increase in expression (C), ii) delayed but progressive increase in expression (D), or iii) an immediate increase in expression that weakens over the time course (E). Notably, all gene clustering's return to sham control expression levels upon TTX cessation and 7-d of recovery.

Figure 6. Relative Fold Change of Gene Expression and DNA Methylation of a Subset of Identified Gene Transcripts Relative fold change in mRNA expression of genes MyoG, Trim 63, Fbxo 32, Chrna 1, Ampd 3 and Hdac 4 (**A -** in descending order). All genes are represented as mean ± standard deviations (n = 6), Ampd3 (n = 3). Statistically significant changes in fold difference compared to sham control group are indicated via *. Sham control group represented with triangle icon. All TTX treated groups represented with square icon

(**A**). Mean methylation data presented as relative fold change compared to control for genes: Myogenin, Trim 63, Fbxo32, Chrna 1 and Ampd 3 (**B -** in descending order). Mean percentage data (black column bars) are the average taken from each CpG island of the respective gene, analysed via loci-specific pyrosequencing. Individual CpG island methylation percentages are visualised as individual lines. DNA methylation data presented as mean ± standard deviation for n = 3. Statistically significant reductions compared to control group are indicated by use of *. § indicates significant reduction compared to 7-d and 14-d TTX atrophy. ✣ indicates a significant reduction in DNA methylation compared to 3-d TTX exposed experimental group (**B**). Finally, an overlap schematic (**C**) is presented to represent the relationship between DNA methylation and mRNA expression of key transcripts (arbitrary units).

Common Abbreviations

CSA, cross-sectional area; H&E, hematoxylin and eosin; TA, tibialis anterior; TTX, tetrodotoxin; nAchR, nicotinic acetyl choline receptor; MyoG, myogenin; Hdac4, Histone Deacetylase 4; Trim63 / Murf1, tripartite motif containing 63 or Muscle RING-finger protein-1; Ampd3, adenosine monophosphate deaminase 3; Chrna1, acetylcholine receptor subunit alpha 1; bHLH muscle specific basic helix-loop-helix; MRFs, myogenic regulatory factors; Fbxo32 / MaFbx, F-Box Protein 32 / muscle-specific F-box protein; HRM, High Resolution Melting

References

1. Ferrando, A. A., Lane, H. W., Stuart, C. A., Davis-Street, J., and Wolfe, R. R. (1996) Prolonged bed rest decreases skeletal muscle and whole body protein synthesis. *The American journal of physiology* **270**, E627-633
2. LeBlanc, A. D., Schneider, V. S., Evans, H. J., Pientok, C., Rowe, R., and Spector, E. (1992) Regional changes in muscle mass following 17 weeks of bed rest. *Journal of applied physiology (Bethesda, Md. : 1985)* **73**, 2172-2178
3. Gibson, J. N., Halliday, D., Morrison, W. L., Stoward, P. J., Hornsby, G. A., Watt, P. W., Murdoch, G., and Rennie, M. J. (1987) Decrease in human quadriceps muscle protein turnover consequent upon leg immobilization. *Clinical science (London, England : 1979)* **72**, 503-509
4. Deitrick, J. E. (1948) The Effect of Immobilization on Metabolic and Physiological Functions of Normal Men. *Bulletin of the New York Academy of Medicine* **24**, 364-375

5. Acharyya, S., Ladner, K. J., Nelsen, L. L., Damrauer, J., Reiser, P. J., Swoap, S., and Guttridge, D. C. (2004) Cancer cachexia is regulated by selective targeting of skeletal muscle gene products. *The Journal of clinical investigation* **114**, 370-378
6. Tan, B. H., and Fearon, K. C. (2008) Cachexia: prevalence and impact in medicine. *Current opinion in clinical nutrition and metabolic care* **11**, 400-407
7. Hasselgren, P. O., and Fischer, J. E. (1998) Sepsis: stimulation of energy-dependent protein breakdown resulting in protein loss in skeletal muscle. *World J Surg* **22**, 203-208
8. Strassburg, S., Springer, J., and Anker, S. D. (2005) Muscle wasting in cardiac cachexia. *The international journal of biochemistry & cell biology* **37**, 1938-1947
9. Kalyani, R. R., Corriere, M., and Ferrucci, L. (2014) Age-related and disease-related muscle loss: the effect of diabetes, obesity, and other diseases. *The lancet. Diabetes & endocrinology* **2**, 819-829
10. Giangregorio, L. (2006) Bone Loss and Muscle Atrophy in Spinal Cord Injury: Epidemiology, Fracture Prediction, and Rehabilitation Strategies. *The Journal of Spinal Cord Medicine* **29**, 489-500
11. Janssen, I., Heymsfield, S. B., and Ross, R. (2002) Low relative skeletal muscle mass (sarcopenia) in older persons is associated with functional impairment and physical disability. *J Am Geriatr Soc* **50**, 889-896
12. Batt, J., Bain, J., Goncalves, J., Michalski, B., Plant, P., Fahnestock, M., and Woodgett, J. (2006) Differential gene expression profiling of short and long term denervated muscle. *FASEB journal : official publication of the Federation of American Societies for Experimental Biology* **20**, 115-117
13. Dupont Salter, A. C., Richmond, F. J., and Loeb, G. E. (2003) Effects of muscle immobilization at different lengths on tetrodotoxin-induced disuse atrophy. *IEEE transactions on neural systems and rehabilitation engineering : a publication of the IEEE Engineering in Medicine and Biology Society* **11**, 209-217
14. de Boer, M. D., Maganaris, C. N., Seynnes, O. R., Rennie, M. J., and Narici, M. V. (2007) Time course of muscular, neural and tendinous adaptations to 23 day unilateral lower-limb suspension in young men. *The Journal of physiology* **583**, 1079-1091
15. Nikawa, T., Ishidoh, K., Hirasaka, K., Ishihara, I., Ikemoto, M., Kano, M., Kominami, E., Nonaka, I., Ogawa, T., Adams, G. R., Baldwin, K. M., Yasui, N., Kishi, K., and Takeda, S. (2004) Skeletal muscle gene expression in space-flown rats. *FASEB journal : official publication of the Federation of American Societies for Experimental Biology* **18**, 522-524
16. Jarvis, J. C., and Salmons, S. (1991) A family of neuromuscular stimulators with optical transcutaneous control. *Journal of medical engineering & technology* **15**, 53-57
17. Jarvis, J. C., Mokrusch, T., Kwende, M. M., Sutherland, H., and Salmons, S. (1996) Fast-to-slow transformation in stimulated rat muscle. *Muscle & nerve* **19**, 1469-1475
18. Bonaldo, P., and Sandri, M. (2013) Cellular and molecular mechanisms of muscle atrophy. *Disease Models & Mechanisms* **6**, 25-39
19. Eddins, M. J., Varadan, R., Fushman, D., Pickart, C. M., and Wolberger, C. (2007) Crystal structure and solution NMR studies of Lys48-linked tetraubiquitin at neutral pH. *Journal of molecular biology* **367**, 204-211

20. Sandri, M., Sandri, C., Gilbert, A., Skurk, C., Calabria, E., Picard, A., Walsh, K., Schiaffino, S., Lecker, S. H., and Goldberg, A. L. (2004) Foxo transcription factors induce the atrophy-related ubiquitin ligase atrogin-1 and cause skeletal muscle atrophy. *Cell* **117**, 399-412
21. Lecker, S. H., Jagoe, R. T., Gilbert, A., Gomes, M., Baracos, V., Bailey, J., Price, S. R., Mitch, W. E., and Goldberg, A. L. (2004) Multiple types of skeletal muscle atrophy involve a common program of changes in gene expression. *Faseb J* **18**, 39-51
22. Jaenisch, R., and Bird, A. (2003) Epigenetic regulation of gene expression: how the genome integrates intrinsic and environmental signals. *Nature genetics* **33 Suppl**, 245-254
23. Magnusson, C., Svensson, A., Christerson, U., and Tagerud, S. (2005) Denervation-induced alterations in gene expression in mouse skeletal muscle. *The European journal of neuroscience* **21**, 577-580
24. Sharples, A. P., Polydorou, I., Hughes, D. C., Owens, D. J., Hughes, T. M., and Stewart, C. E. (2016) Skeletal muscle cells possess a 'memory' of acute early life TNF-alpha exposure: role of epigenetic adaptation. *Biogerontology* **17**, 603-617
25. Sharples, A. P., Stewart, C. E., and Seaborne, R. A. (2016) Does skeletal muscle have an 'epi'-memory? The role of epigenetics in nutritional programming, metabolic disease, aging and exercise. *Aging cell* **15**, 603-616
26. Ehrlich, K. C., Paterson, H. L., Lacey, M., and Ehrlich, M. (2016) DNA Hypomethylation in Intragenic and Intergenic Enhancer Chromatin of Muscle-Specific Genes Usually Correlates with their Expression. *The Yale Journal of Biology and Medicine* **89**, 441-455
27. Buffelli, M., Pasino, E., and Cangiano, A. (1997) Paralysis of rat skeletal muscle equally affects contractile properties as does permanent denervation. *Journal of muscle research and cell motility* **18**, 683-695
28. Michel, R. N., and Gardiner, P. F. (1990) To what extent is hindlimb suspension a model of disuse? *Muscle & nerve* **13**, 646-653
29. Irizarry, R. A., Bolstad, B. M., Collin, F., Cope, L. M., Hobbs, B., and Speed, T. P. (2003) Summaries of Affymetrix GeneChip probe level data. *Nucleic acids research* **31**, e15
30. Irizarry, R. A., Hobbs, B., Collin, F., Beazer-Barclay, Y. D., Antonellis, K. J., Scherf, U., and Speed, T. P. (2003) Exploration, normalization, and summaries of high density oligonucleotide array probe level data. *Biostatistics (Oxford, England)* **4**, 249-264
31. Schmittgen, T. D., and Livak, K. J. (2008) Analyzing real-time PCR data by the comparative CT method. *Nature Protocols* **3**, 1101-1108
32. Davis, P., Witczak, C., and Brault, J. (2015) AMP Deaminase 3 Accelerates Protein Degradation in C2C12 Myotubes. *The FASEB Journal* **29**
33. Cohen, S., Brault, J. J., Gygi, S. P., Glass, D. J., Valenzuela, D. M., Gartner, C., Latres, E., and Goldberg, A. L. (2009) During muscle atrophy, thick, but not thin, filament components are degraded by MuRF1-dependent ubiquitylation. *The Journal of cell biology* **185**, 1083-1095
34. Cohen, T. J., Waddell, D. S., Barrientos, T., Lu, Z., Feng, G., Cox, G. A., Bodine, S. C., and Yao, T. P. (2007) The histone deacetylase HDAC4 connects neural activity to muscle transcriptional reprogramming. *The Journal of biological chemistry* **282**, 33752-33759
35. Tang, H., and Goldman, D. (2006) Activity-dependent gene regulation in skeletal muscle is mediated by a histone deacetylase (HDAC)-Dach2-myogenin signal

transduction cascade. *Proceedings of the National Academy of Sciences of the United States of America* **103**, 16977-16982
36. Tang, H., Macpherson, P., Marvin, M., Meadows, E., Klein, W. H., Yang, X. J., and Goldman, D. (2009) A histone deacetylase 4/myogenin positive feedback loop coordinates denervation-dependent gene induction and suppression. *Molecular biology of the cell* **20**, 1120-1131
37. Tang, W. W., Dietmann, S., Irie, N., Leitch, H. G., Floros, V. I., Bradshaw, C. R., Hackett, J. A., Chinnery, P. F., and Surani, M. A. (2015) A Unique Gene Regulatory Network Resets the Human Germline Epigenome for Development. *Cell* **161**, 1453-1467
38. Macpherson, P. C. D., Wang, X., and Goldman, D. (2011) Myogenin Regulates Denervation-Dependent Muscle Atrophy in Mouse Soleus Muscle. *J Cell Biochem* **112**, 2149-2159
39. Moresi, V., Williams, A. H., Meadows, E., Flynn, J. M., Potthoff, M. J., McAnally, J., Shelton, J. M., Backs, J., Klein, W. H., Richardson, J. A., Bassel-Duby, R., and Olson, E. N. (2010) Myogenin and class II HDACs control neurogenic muscle atrophy by inducing E3 ubiquitin ligases. *Cell* **143**, 35-45
40. Yu, X. M., and Hall, Z. W. (1991) Extracellular domains mediating epsilon subunit interactions of muscle acetylcholine receptor. *Nature* **352**, 64-67
41. Ibebunjo, C., Chick, J. M., Kendall, T., Eash, J. K., Li, C., Zhang, Y., Vickers, C., Wu, Z., Clarke, B. A., Shi, J., Cruz, J., Fournier, B., Brachat, S., Gutzwiller, S., Ma, Q., Markovits, J., Broome, M., Steinkrauss, M., Skuba, E., Galarneau, J. R., Gygi, S. P., and Glass, D. J. (2013) Genomic and proteomic profiling reveals reduced mitochondrial function and disruption of the neuromuscular junction driving rat sarcopenia. *Molecular and cellular biology* **33**, 194-212
42. Llano-Diez, M., Gustafson, A.-M., Olsson, C., Goransson, H., and Larsson, L. (2011) Muscle wasting and the temporal gene expression pattern in a novel rat intensive care unit model. *BMC Genomics* **12**, 602
43. Bogdanovic, O., and Veenstra, G. J. (2009) DNA methylation and methyl-CpG binding proteins: developmental requirements and function. *Chromosoma* **118**, 549-565
44. Reik, W., Dean, W., and Walter, J. (2001) Epigenetic reprogramming in mammalian development. *Science (New York, N.Y.)* **293**, 1089-1093
45. Barres, R., Yan, J., Egan, B., Treebak, J. T., Rasmussen, M., Fritz, T., Caidahl, K., Krook, A., O'Gorman, D. J., and Zierath, J. R. (2012) Acute exercise remodels promoter methylation in human skeletal muscle. *Cell Metab* **15**, 405-411
46. Trasler, J., Deng, L., Melnyk, S., Pogribny, I., Hiou-Tim, F., Sibani, S., Oakes, C., Li, E., James, S. J., and Rozen, R. (2003) Impact of Dnmt1 deficiency, with and without low folate diets, on tumor numbers and DNA methylation in Min mice. *Carcinogenesis* **24**, 39-45
47. Jacobsen, S. C., Brons, C., Bork-Jensen, J., Ribel-Madsen, R., Yang, B., Lara, E., Hall, E., Calvanese, V., Nilsson, E., Jorgensen, S. W., Mandrup, S., Ling, C., Fernandez, A. F., Fraga, M. F., Poulsen, P., and Vaag, A. (2012) Effects of short-term high-fat overfeeding on genome-wide DNA methylation in the skeletal muscle of healthy young men. *Diabetologia* **55**, 3341-3349
48. Le Grand, F., and Rudnicki, M. A. (2007) Skeletal muscle satellite cells and adult myogenesis. *Curr Opin Cell Biol* **19**, 628-633

876 49. Bodine, S. C., and Baehr, L. M. (2014) Skeletal muscle atrophy and the E3 ubiquitin
877 ligases MuRF1 and MAFbx/atrogin-1. *American journal of physiology. Endocrinology*
878 *and metabolism* **307**, E469-484
879 50. Bodine, S. C., Latres, E., Baumhueter, S., Lai, V. K., Nunez, L., Clarke, B. A.,
880 Poueymirou, W. T., Panaro, F. J., Na, E., Dharmarajan, K., Pan, Z. Q., Valenzuela, D.
881 M., DeChiara, T. M., Stitt, T. N., Yancopoulos, G. D., and Glass, D. J. (2001)
882 Identification of ubiquitin ligases required for skeletal muscle atrophy. *Science* **294**,
883 1704-1708
884 51. Goldberg, A. L. (1969) Protein turnover in skeletal muscle. II. Effects of denervation
885 and cortisone on protein catabolism in skeletal muscle. *The Journal of biological*
886 *chemistry* **244**, 3223-3229
887 52. Giniatullin, R., Nistri, A., and Yakel, J. L. (2005) Desensitization of nicotinic ACh
888 receptors: shaping cholinergic signaling. *Trends in neurosciences* **28**, 371-378
889 53. Beker, F., Weber, M., Fink, R. H., and Adams, D. J. (2003) Muscarinic and nicotinic
890 ACh receptor activation differentially mobilize Ca2+ in rat intracardiac ganglion
891 neurons. *Journal of neurophysiology* **90**, 1956-1964
892 54. Ibebunjo, C. (2013) Genomic and Proteomic Profiling Reveals Reduced Mitochondrial
893 Function and Disruption of the Neuromuscular Junction Driving Rat Sarcopenia. **33**,
894 194-212
895 55. Colquhoun, D., and Sivilotti, L. G. (2004) Function and structure in glycine receptors
896 and some of their relatives. *Trends in neurosciences* **27**, 337-344
897

Table 1. Primer Assay Design for Reverse Transcription Quantitative Real Time Polymerase Chain Reaction

Gene Name	Accession No.		Primer Sequence	Primer Length	Optimum Annealing Temperature	Product Length
Trim63	NM_080903	F	GGAGGAGTTTACTGAAGAGG	20	61	180
		R	GACACACTTCCCTATGGTGC	20		
Fbxo32	NM_133521	F	CTTGTCTGACAAAGGGCAGC	20	61	184
		R	TGAAAGTGAGACGGAGCAGC	20		
Ampd3	NM_031544	F	ACGCTTGCTGGTCGGTTTAG	20	60	96
		R	TGGCTTCCTTCTGTCCGATG	20		
Hdac4	XM_343629.4	F	GCAGCCAAACTTCTCCAGCA	20	61	212
		R	TTGACATTGAAACCCACGCC	20		
MyoG	NM_017115.2	F	GCCATCCAGTACATTGAGCG	20	61	267
		R	CATATCCTCCACCGTGATGC	20		
Chrna1	NM_024485.1	F	TGTCATCAACACACACCACC	20	61	269
		R	CTGCAATGTACTTCACACCC	20		

Table 2. Description of targeted DNA methylation assays for loci specific pyrosequencing analysis

Gene	CpG	Position from ATG codon	Position from TSS	Chromatin Location	Assay Sequence
Myogenin		-280 to -251	-247 to -218	**Chr13:** 51126212-51126241	AGTYGAYGGTTTTTYGATTYGTGTAT AGGAGTYGTTTGGG
	CpG-9	-280	-247	Chr13:51126212	
	CpG-8	-277	-244	Chr13:51126215	
	CpG-7	-269	-236	Chr13:51126223	
	CpG-6	-264	-231	Chr13:51126228	
	CpG-5	-251	-218	Chr13:51126241	
Trim 63		-63 to +30	+40 to +133	**Chr5:** 152533388-152533481	ATTYGAGTGGGATTTTTTTTATTYGG TGTGAYGTAGGTGGAAGAGATAGTY GTAGTTTYGAAGTAATATGGATTATA AATTTGGTTTGATTTYGGAYGGAAAT G
	CpG-5	-64	40	Chr5:152533388	
	CpG-4	-44	60	Chr5:152533408	
	CpG-3	-36	68	Chr5:152533416	
	CpG-2	-17	87	Chr5:152533435	
	CpG-1	-9	95	Chr5:152533443	
	CpG1	26	129	Chr5:152533447	
	CpG2	30	133	Chr5:152533481	
Ampd 3		-559 to -555	-540 to -536	**Chr1:**175585557-175585561	GYGGGYGTATGGGTG
	CpG-10	-559	-540	Chr1:175585557	
	CpG-9	-555	-536	Chr1:175585561	
Fbxo 32		-519 to -465	-322 to -268	**Chr7:** 98098536-98098590	TAYGTTYGATAGGGGAGTAGGGGA GGTGTAAGAGGTGTTAGGGTATYGA GGGTTAGYGGGATATTTGG
	CpG-49	-519	-322	Chr7:98098590	
	CpG-48	-515	-318	Chr7:98098586	
	CpG-47	-475	-278	Chr7:98098546	
	CpG-46	-465	-268	Chr7:98098536	
Chrna 1		-198 to -240	-137 to -179	**Chr3:** 60460861-60460903	TCRACTCATATTAAACRTAAACCRTA TAAAAATCTACATAAATCRTAAACCA AAAAC
	CpG-7	-240	-179	Chr3:60460903	
	CpG-6	-219	-158	Chr3:60460882	
	CpG-5	-212	-151	Chr3:60460875	
	CpG-4	-198	-137	Chr3:60460861	

Table 3. HDAC4 DNA Methylation via High Resolution Melting Polymerase Chain Reaction

Gene Name	CpG No.	Gene Globe Cat No.	Chromatin Location	Primer Sequence	Product Length
Hdac4	1	PM00599046	Chr9:91389151-91391341	GGGCGCGCAAGAGCGCAGACTGTGACGGGGGCCCGGT	190
	2	PM00599053	Chr9:91390077-91391147	GCGCCCGCGAAGCGGGGGTGGCTGTTGGGCTATTGTAGGGCGGA	138
	3	PM00599060	Chr9:91389052-91391220	GCTAGCGCCTGGAGAGTCCTCGGTACGCCCCGC	168
	4	PM00599067	Chr9:91389477-91391621	GCTTTGGGTCGCCGCCACCGCGTCCCGGT	144
	5	PM00599074	Chr9:91389472-91391621	CGTTGCTGTGGCGGAGGTGTAGGCTTTGGGTCGCCGCCACCGCGTCCCG	149

Figure 1

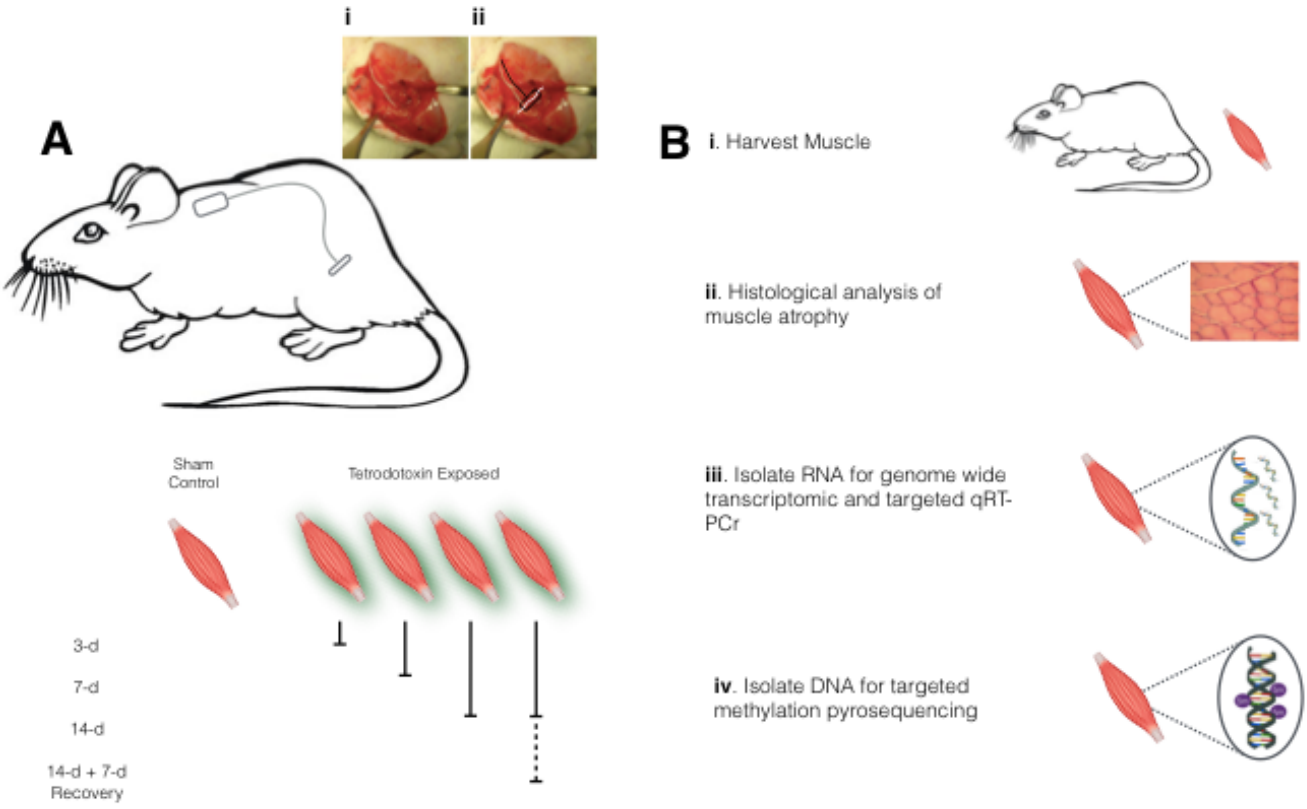
A
i
ii
Sham Control
Tetrodotoxin Exposed
3-d
7-d
14-d
14-d + 7-d Recovery
B
i. Harvest Muscle
ii. Histological analysis of muscle atrophy
iii. Isolate RNA for genome wide transcriptomic and targeted qRT-PCr
iv. Isolate DNA for targeted methylation pyrosequencing

Figure 2

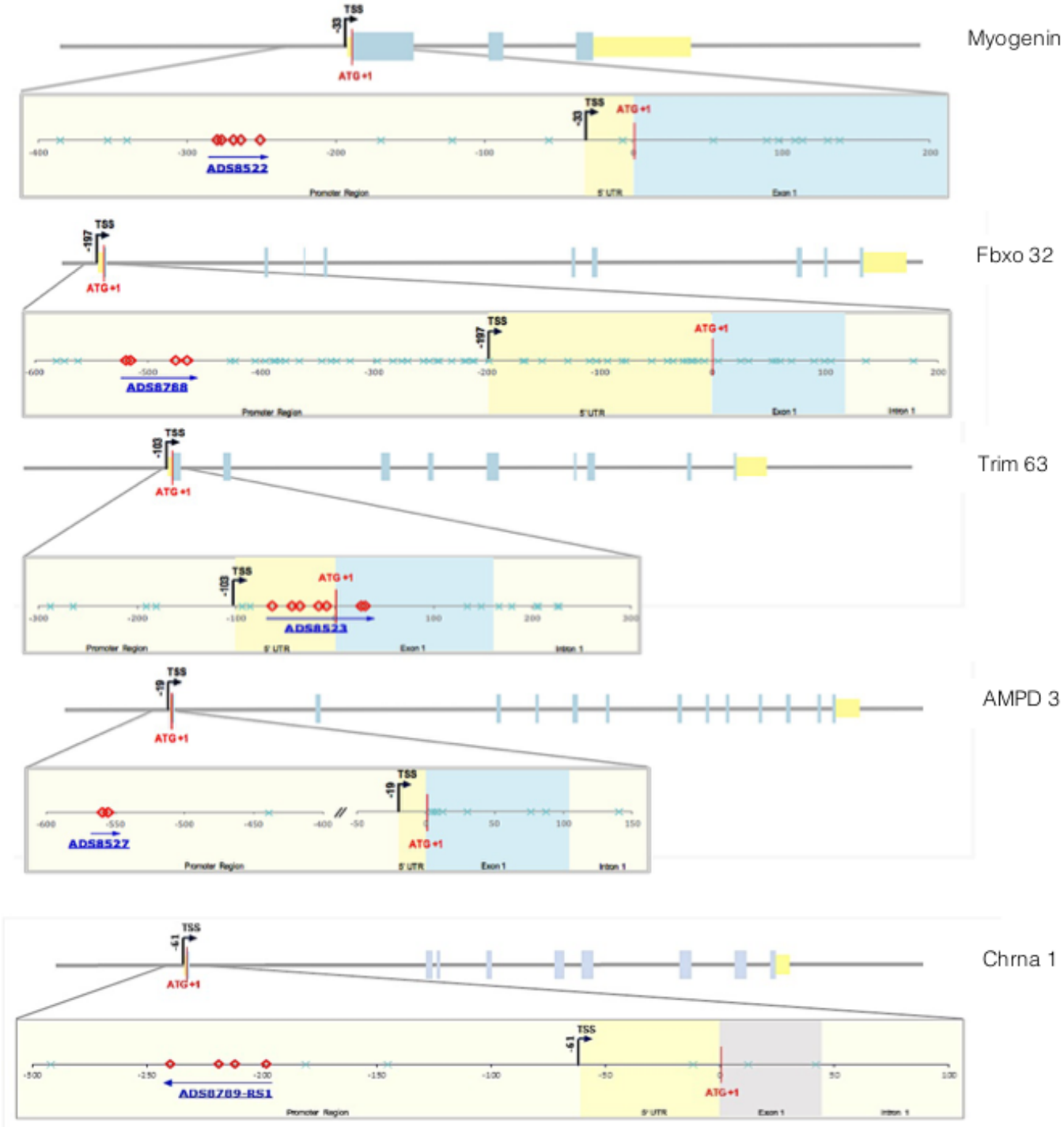
Myogenin
TSS
-33
ATG+1
ADS8522
Promoter Region
5' UTR
Exon 1
Fbxo 32
-197
ADS8788
Intron 1
Trim 63
-103
ADS8523
AMPD 3
-19
ADS8527
Chrna 1
-61
ADS8789-RS1
TSS : Transcriptional Start Site
: CpG site analyzed
: CpG site not analyzed
: Exon coding region
: 5' or 3' (UTR)
: Simplex Assay

Figure 3

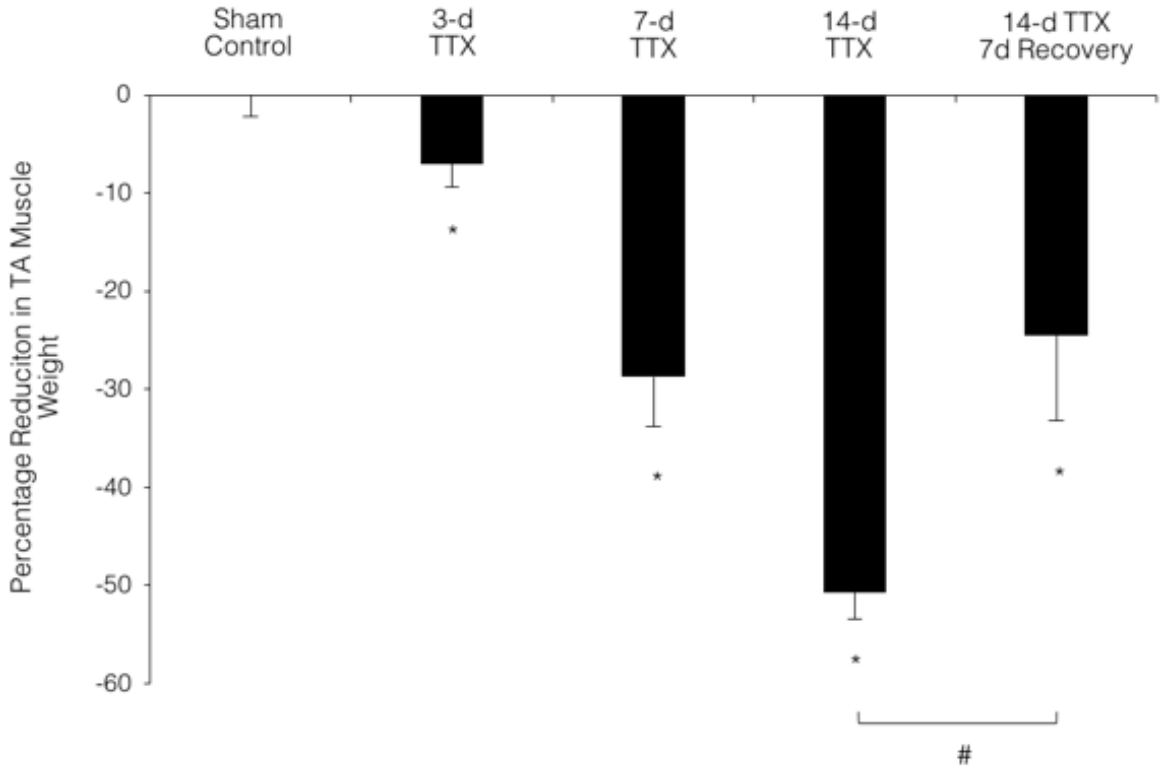
Sham Control
3-d TTX
7-d TTX
14-d TTX
14-d TTX 7d Recovery
Percentage Reduciton in TA Muscle Weight
0
-10
-20
-30
-40
-50
-60
*
*
*
*
#

Figure 4

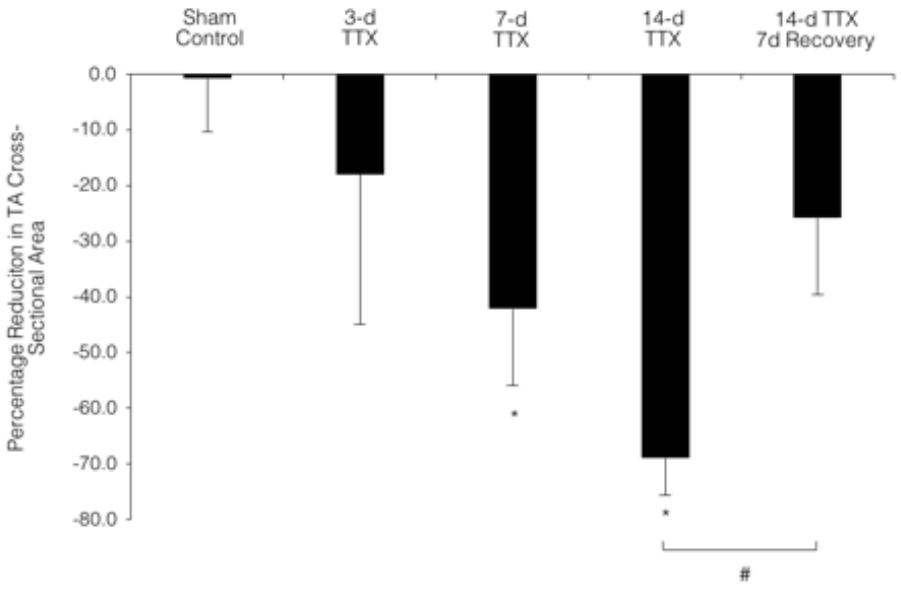
Sham Control
3-d TTX
7-d TTX
14-d TTX
14-d TTX 7d Recovery
Percentage Reduciton in TA Cross-Sectional Area
0.0
-10.0
-20.0
-30.0
-40.0
-50.0
-60.0
-70.0
-80.0
*
*
#

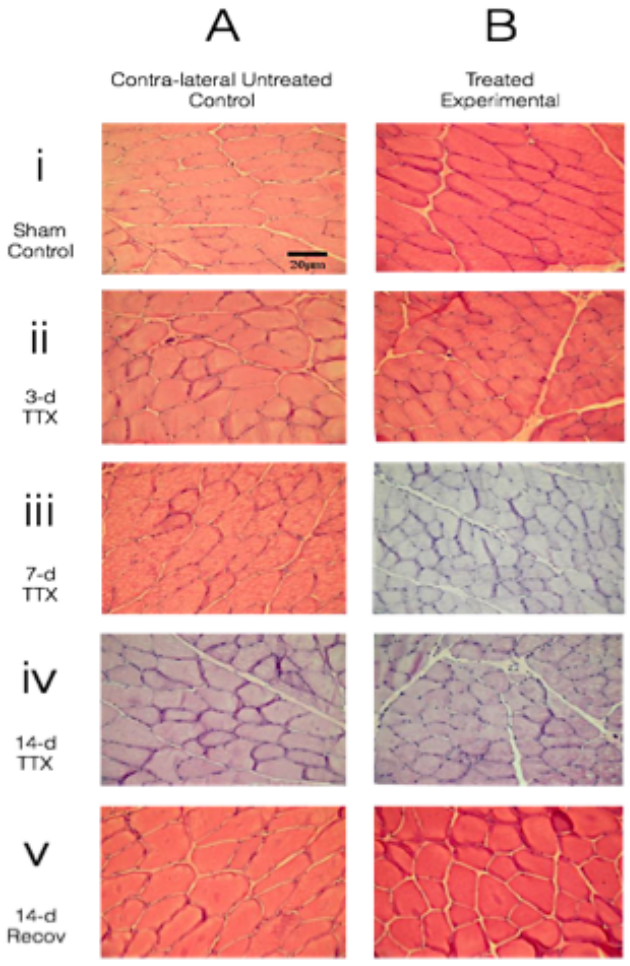
A
B
Contra-lateral Untreated Control
Treated Experimental
i
Sham Control
ii
3-d TTX
iii
7-d TTX
iv
14-d TTX
v
14-d Recov

Figure 5

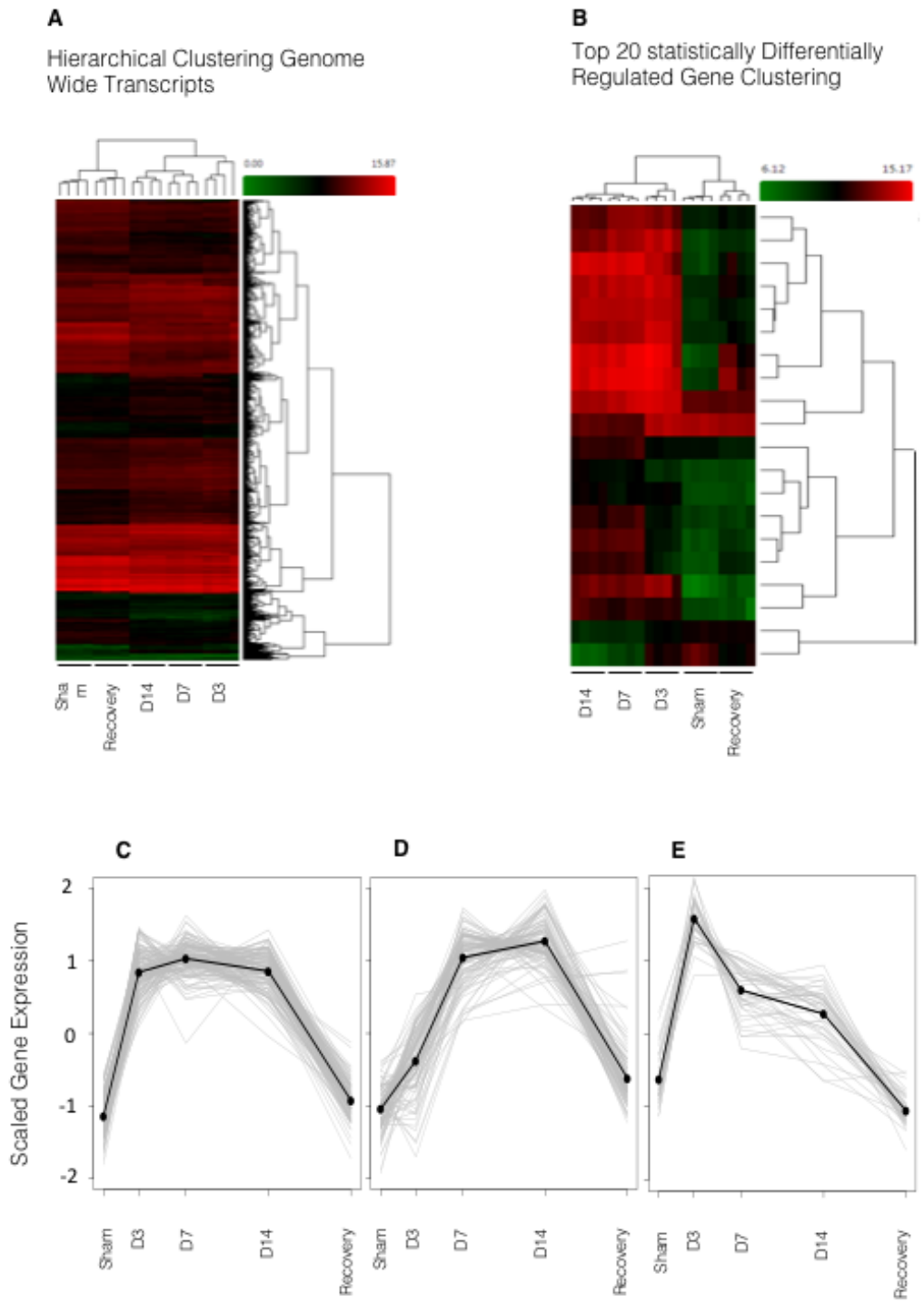
A
Hierarchical Clustering Genome Wide Transcripts
0.00
15.87
Sham
Recovery
D14
D7
D3
B
Top 20 statistically Differentially Regulated Gene Clustering
6.12
15.17
D14
D7
D3
Sham
Recovery
C
D
E
Scaled Gene Expression
2
1
0
-1
-2
Sham
D3
D7
D14
Recovery

Figure 6

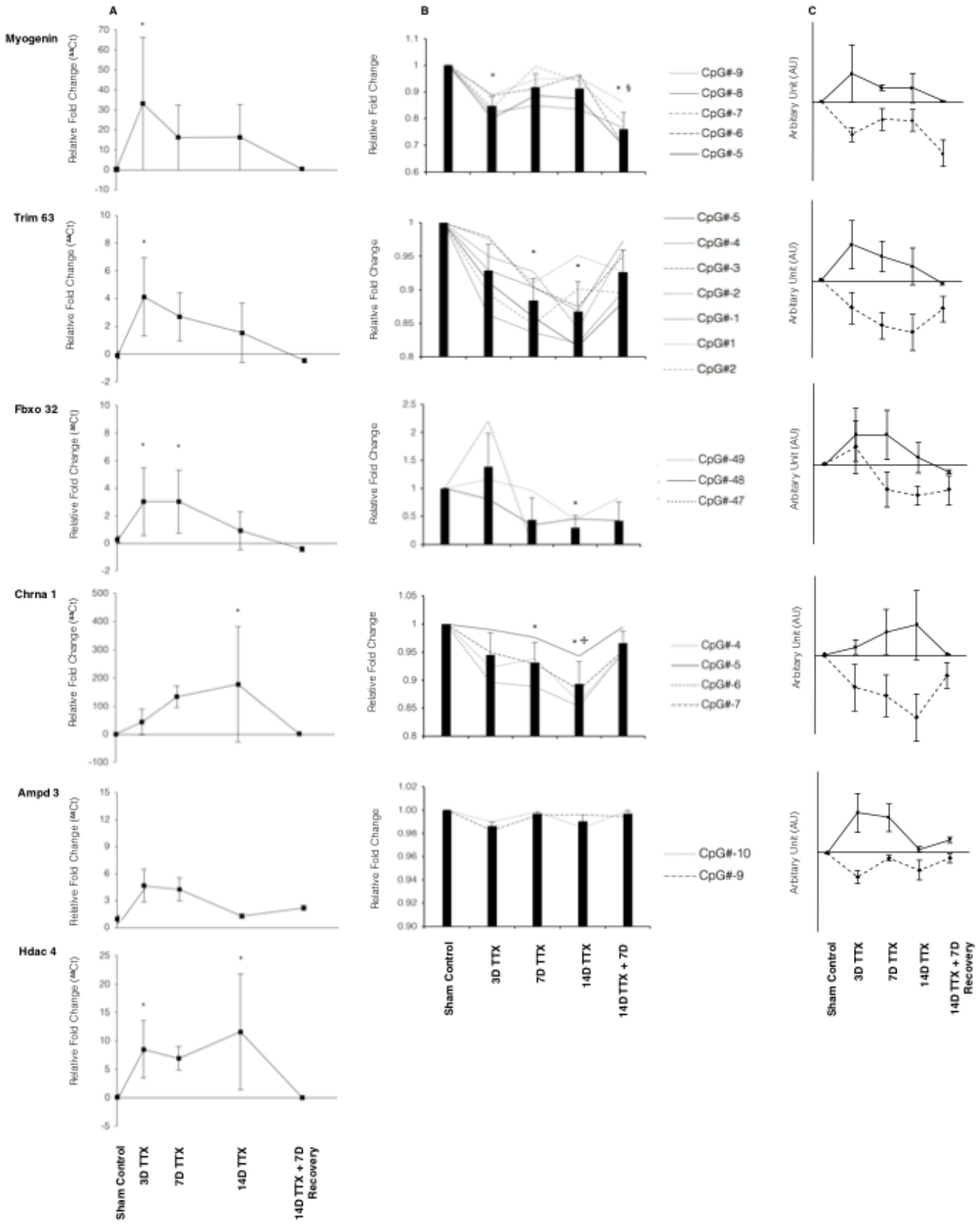
A
B
C
Myogenin
Trim 63
Fbxo 32
Chrna 1
Ampd 3
Hdac 4
Relative Fold Change (ΔΔCt)
Relative Fold Change
Arbitary Unit (AU)
CpG#-9
CpG#-8
CpG#-7
CpG#-6
CpG#-5
CpG#-4
CpG#-3
CpG#-2
CpG#-1
CpG#1
CpG#2
CpG#-49
CpG#-48
CpG#-47
CpG#-10
Sham Control
3D TTX
7D TTX
14D TTX
14D TTX + 7D
14D TTX + 7D Recovery